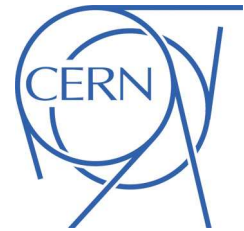# ATLAS NOTE

ATLAS-CONF-2012-070

June 27, 2012

Search for light top squark pair production in final states with leptons and b-jets with the ATLAS detector in $\sqrt{s} = 7$ TeV proton–proton collisions

The ATLAS Collaboration

Abstract

The results of a search for pair production of light top squarks are presented, using 4.7 fb^{-1} of $\sqrt{s} = 7$ TeV proton–proton collisions with the ATLAS detector at the Large Hadron Collider. This search targets top squarks with masses similar to, or lighter than, the top quark mass. Final states containing exclusively one or two leptons (e, μ), large missing transverse momentum, light flavour jets and b-jets are used to reconstruct the top squark pair system. Global mass scale variables are used to separate the signal from a large $t\bar{t}$ background. No excess over the Standard Model expectation is found. The results are interpreted in the framework of the minimal supersymmetric Standard Model, assuming the top squark decays exclusively to a chargino and a b-quark. Light top squarks with masses from 120 GeV up to the top mass are excluded for neutralino masses around 55 GeV.

1 Introduction

Supersymmetry (SUSY) [1–9] is an extension of the Standard Model (SM) which naturally resolves the hierarchy problem by introducing supersymmetric partners to the known fermions and bosons. In the framework of a generic R-parity conserving minimal supersymmetric extension of the SM (MSSM) [10–14], SUSY particles are produced in pairs and the lightest supersymmetric particle (LSP) is stable. In a large variety of models the LSP is the lightest neutralino, $\tilde{\chi}_1^0$, which only interacts weakly. The scalar partners of right-handed and left-handed quarks (squarks) can mix to form two mass eigenstates ($\tilde{q}_1, \tilde{q}_2$). Large mixing in the third generation sector can yield top squarks (stop, $\tilde{t}_{1,2}$) with one of the mass eigenstates significantly lighter than the other squarks. In particular, the lightest stop, $\tilde{t}_1$, could have a mass similar to, or lower than, the top quark mass, as favoured by Electroweak Baryogenesis MSSM scenarios [15, 16].

In this letter, a search for direct stop pair production is presented targeting these scenarios. A SUSY particle mass hierarchy is assumed such that $m_t \gtrsim m_{\tilde{t}_1} > m_{\tilde{\chi}_1^\pm}$ and that the stop decays exclusively into a b-quark and chargino ($\tilde{t}_1 \to \tilde{\chi}_1^\pm b$). The chargino subsequently decays via a virtual or real W boson ($\tilde{\chi}_1^\pm \to W^{(*)} \tilde{\chi}_1^0$). The masses of all other supersymmetric particles are assumed to be above the TeV scale, and large stop gauge mixing results in $m_{\tilde{t}_2} \gg m_{\tilde{t}_1}$. In the case where $m_{\tilde{t}_1} \sim m_t$, direct stop pair production will lead to final states very similar to SM $t\bar{t}$ events, which form the dominant background. In the first stage of the analysis the $t\bar{t}$ system (including stop pairs) is reconstructed from final states which contain exclusively one or two leptons ($\ell = e, \mu$), b-jets, light flavour jets, and large missing transverse momentum. The use of global mass scale variables allows discrimination between stop pairs and the $t\bar{t}$ background. The results are interpreted in three MSSM scenarios where stop and neutralino masses are varied and different assumptions are made about the chargino-neutralino mass difference: gaugino universality ($m_{\tilde{\chi}_1^\pm} \simeq 2 \times m_{\tilde{\chi}_1^0}$); fixed chargino mass at 106 GeV (above the present exclusion limit from LEP [17]); and fixed stop mass of 180 GeV with variations of the chargino-neutralino mass difference. Previous results on direct production of top squark pairs in the same MSSM scenarios have been presented by the CDF [18] and ATLAS collaborations [19].

2 The ATLAS Detector

The ATLAS detector is described in detail elsewhere [20]. It comprises an inner detector (ID) surrounded by a thin superconducting solenoid, a calorimeter system and an extensive muon spectrometer embedded in a toroidal magnetic field. The ID tracking system consists of a silicon pixel detector, a silicon microstrip detector (SCT), and a transition radiation tracker (TRT). It provides tracking information for charged particles in a pseudorapidity[1] range $|\eta| < 2.5$ and allows for efficient identification of jets originating from b-hadron decays using impact parameter measurements to reconstruct secondary decay vertices. The ID is immersed in a 2 T axial magnetic field and is surrounded by high-granularity liquid-argon sampling electromagnetic calorimeters. An iron-scintillator tile calorimeter provides hadronic energy measurments in the central rapidity range. In the forward regions, it is complemented by two end-cap calorimeters using liquid argon as the active material and copper or tungsten as an absorber. The muon spectrometer (MS) surrounds the calorimeters and consists of three large superconducting eight-coil

---

[1]ATLAS uses a right-handed coordinate system with its origin at the nominal interaction point (IP) in the centre of the detector, with the z-axis coinciding with the beam pipe axis. The x-axis points from the IP to the centre of the LHC ring, and the y-axis points upwards. Cylindrical coordinates (r, ϕ) are used in the transverse plane, ϕ being the azimuthal angle around the beam pipe. The pseudorapidity is defined in terms of the polar angle θ as $\eta = -\ln\tan(\theta/2)$. The distance ΔR in the $\eta - \phi$ space is defined as $\Delta R = \sqrt{(\Delta\eta)^2 + (\Delta\phi)^2}$.

toroids, a system of tracking chambers, and detectors for triggering.

3   Simulated Event Samples

Monte Carlo (MC) simulated event samples are used to develop and validate the analysis procedure and to help evaluate the SM backgrounds in the signal regions. Production of top quark pairs is simulated with MC@NLO [21], using a top quark mass of 172.5 GeV and the next-to-leading order (NLO) parton distribution functions (PDF) CTEQ6.6 [22], which are used with all NLO MC codes in this analysis. Samples of W and Z/γ^* production, with accompanying light and heavy flavour jets, and $t\bar{t}$ with additional b-jets ($t\bar{t}b\bar{b}$) are generated using ALPGEN [23]. Samples of $Zt\bar{t}$, $Wt\bar{t}$ and $WWt\bar{t}$ are generated with MADGRAPH [24] interfaced to PYTHIA [25]. Diboson (WW, WZ, ZZ) production is generated with HERWIG [26] and single top production with MC@NLO for the s- and $t+W$ channels, and AcerMC [27] for the t-channel. Fragmentation and hadronisation modelling for the ALPGEN and MC@NLO samples are performed by HERWIG, using JIMMY [28] for the underlying event. ALPGEN and POWHEG [29] samples are used to assess the systematic uncertainties associated with the choice of generator for $t\bar{t}$ production, and AcerMC samples are used to assess the uncertainties associated with initial and final state radiation (ISR/FSR). The choice of PDF depends on the generator. MRST2007 LO [30] sets are used for HERWIG, CTEQ6L1 [31] with ALPGEN. The background predictions are normalised to the theoretical cross sections, including higher-order QCD corrections when available, as detailed in Ref. [32].

Direct stop pair production samples are generated using PYTHIA6 and HERWIG++ [33]. Signal cross sections are calculated to NLO in the strong coupling constant, including the resummation of soft gluon emission at next-to-leading-logarithmic accuracy (NLO + NLL) [34–36]. The nominal cross section and the uncertainty are taken from an envelope of cross section predictions using different PDF sets and factorisation and renormalisation scales, as described in Ref. [37].

All MC samples are produced using the ATLAS MC11c parameter tune [38] and a GEANT4 [39] based detector simulation [40]. MC samples are re-weighted such that the number of additional proton–proton interactions per bunch crossing (pile-up) agrees with that expected in data.

4   Object Reconstruction

Electron candidates are reconstructed from energy clusters in the electromagnetic calorimeters matched to a track in the ID. They are required to have $p_T > 20$ GeV, $|\eta| < 2.47$ and to pass the "medium" shower shape and track selection criteria of Ref. [41].

Muons are reconstructed using an algorithm [42] that combines information from the ID and MS. Candidate muons are required to have $p_T > 10$ GeV, $|\eta| < 2.4$, and be reconstructed with a sufficient number of hits in the pixel, SCT and TRT detectors. In order to reject muons originating from cosmic rays, events containing muon candidates with a distance of closest approach of greater than 1 mm to the primary vertex in the z direction, or an impact parameter of greater than 0.2 mm, are rejected. The primary vertex itself is defined as the vertex with the highest summed track p_T^2.

Jet candidates are reconstructed using the anti-k_t jet clustering algorithm [43] with a distance parameter of $R = 0.4$. The measured jet energy is corrected for inhomogeneities and for the non-compensating nature of the calorimeter using p_T and η dependent correction factors based on MC simulation validated with extensive test-beam and collision-data studies. Furthermore,

the reconstructed jet is modified such that its direction points to the primary vertex and events containing jets likely to have arisen from detector noise or cosmic rays are rejected [44]. Only jet candidates with corrected transverse momenta $p_T > 20$ GeV and $|\eta| < 4.5$ are retained.

Following object reconstruction, candidate jets and leptons may point to the same energy deposits in the calorimeter. These overlaps are resolved by first discarding any jet candidates within $\Delta R < 0.2$ of an electron. Then, any electron or muon candidate remaining within $\Delta R < 0.4$ of any surviving jet is also discarded.

The missing transverse momentum two-vector, $\mathbf{p}_T^{miss}$, and its magnitude E_T^{miss}, are computed from the negative of the vector sum of the p_T of the reconstructed electrons, muons and jets, and all calorimeter clusters with $|\eta| < 4.9$ not associated with such objects.

Following the overlap removal, electrons must additionally pass the "tight" electron criteria of Ref. [41], and be isolated such that the scalar p_T sum of tracks within a cone of $\Delta R < 0.2$ around the electron candidate (not including the electron track) must be less than 10% of the electron p_T. Muons must also be isolated such that the p_T sum of tracks (not including the muon track) within $\Delta R < 0.2$ is less than 1.8 GeV. Jets are further required to lie within $|\eta| < 2.5$ and have a reasonably high fraction of track p_T associated with the primary vertex. This reduces the presence of jets arising from uncorrelated soft collisions (pile-up) and discards jets without reconstructed tracks.

A b-tagging algorithm [45] is used to identify jets containing a b-hadron decay. The algorithm uses a multivariate technique based on the properties of the secondary vertex, of tracks within the jet, and of the jet itself. The nominal b-tagging efficiency, computed on $t\bar{t}$ MC events, is on average 60%, with a misidentification (mis-tag) rate for c-quark (light-quark/gluon) jets of less than 10% (1%).

5 Event Selection

Application of beam, detector and data-quality requirements gives a total integrated luminosity of 4.7 ± 0.2 fb^{-1}, measured as described in Refs. [46, 47]. The data are selected with a three-level trigger system used to select single lepton events, using requirements that vary with the data-taking period. The tightest electron trigger has an efficiency of $\sim$97% for electrons with $p_T > 25$ GeV. The equivalent muon trigger reaches an efficiency plateau of $\sim$75% ($\sim$90%) in the barrel (end-caps) for muons with $p_T > 20$ GeV. Collision events are selected by requiring a reconstructed vertex with at least five associated tracks, consistent with the beam spot position. Two signal regions are defined containing either exclusively one or two charged leptons ($\ell = e, \mu$) in the final state, hereafter referred to as the 1- and 2-lepton channels respectively.

In the 1-lepton channel, events are required to contain the minimum number of objects expected from the semi-leptonic decay of the $t\bar{t}$ system. Exactly one lepton is required, which must have $p_T > 25$ GeV (20 GeV) for the electron (muon) channel and fulfill the trigger requirements. Events with an additional electron (muon) with $p_T > 20$ GeV (10 GeV) are rejected to ensure no events are selected by both the 1- and 2-lepton channels. A minimum of four jets is required in the event, at least two of which must pass the b-tagging requirements and at least two must fail them. Events are required to have a missing transverse momentum of $E_T^{miss} > 40$ GeV. Background from multi-jet processes, in which jets are misidentified as leptons, is rejected by requiring that the transverse mass (m_T) of the lepton and E_T^{miss} is larger than 30 GeV.

The invariant mass of the hadronic top decay products (m_t^{had}) is used as an additional discriminating variable. In scenarios where the stop is lighter than the top, m_t^{had} will tend to be lower than for background $t\bar{t}$ processes, as illustrated in Fig. 1(a). Since there is an ambiguity as to which b-jet arises from the hadronic top decay (and additional ambiguities at higher

jet multiplicities), the hadronic decay products are tagged using the following algorithm: for every possible combination of light and b-tagged jets in the event, the invariant masses m_W^{had} ($= m_{jj}$), m_W^{lep} (assuming that the lepton and E_T^{miss} arise from the $W \to \ell\nu$ decay), m_t^{had} and m_t^{lep} (the leptonic top mass) are calculated. A top estimator of $P_{\text{tot}} = P(m_W^{\text{had}})P(m_W^{\text{lep}})P(m_t^{\text{lep}})P(m_t^{\text{had}})$ is assigned to this combination, where $P(m)$ is related to the probability for reconstructing a particle of mass m, assuming a Gaussian probability density function with mean values taken from Ref. [48] and experimentally measured widths. The combination which maximises P_{tot} is used to assign one b-jet and two light flavour jets (one b-jet, the lepton and E_T^{miss}) as arising from the hadronic (leptonic) decay of the top quark. Events are then required to have $m_t^{\text{had}} < \hat{\mu} - 0.5\hat{\sigma}$, where $\hat{\mu}$ and $\hat{\sigma}$ are the mean and width respectively of a Gaussian fit to the m_t^{had} distribution in a 40 GeV window around the top mass. This approach is taken to reduce some of the systematic uncertainties, as detailed in Section 6.

In the 2-lepton channel, the following requirements are imposed to ensure that the event contains the required number of objects consistent with the di-leptonic decay of the $t\bar{t}$ system. Exactly two oppositely-charged leptons are required which pass the selection described in Section 4. For same-flavour pairs, the highest p_T lepton is required to have $p_T > 25$ GeV (20 GeV) for electrons (muons). In the case of different flavour pairs, either the electron must have $p_T > 25$ GeV or the muon $p_T > 20$ GeV. At least two jets are required in the event, of which the two with highest p_T are assumed to originate from the $t\bar{t}$ process. At least one of these two jets is required to be b-tagged. The event is required to fulfill $E_T^{\text{miss}} > 40$ GeV and the invariant mass of the two leptons ($m_{\ell\ell}$) must satisfy $30 < m_{\ell\ell} < 81$ GeV.

In order to distinguish between stop and top pair production the mass scale subsystem variable $\sqrt{s_{min}^{(sub)}}$ [49] is employed. The variable is constructed by dividing an event topology into a subsystem comprising both visible and invisible particles originating from the process of interest. The remaining visible particles are labeled as coming from upstream processes such as the underlying event or ISR. With these definitions, the minimum invariant mass compatible with the subsystem is:

$$
\sqrt{s_{min}^{(sub)}} = \left\{ \left(\sqrt{m_{(sub)}^2 + p_{T(sub)}^2} + \sqrt{(m^{\text{miss}})^2 + \left(E_T^{\text{miss}}\right)^2} \right)^2 \right.
$$
$$
\left. - \left(\mathbf{p}_{T(sub)} + \mathbf{p}_T^{\text{miss}} \right)^2 \right\}^{\frac{1}{2}},
$$

(1)

where $m_{(sub)}$ and $p_{T(sub)}$ are the invariant mass and the transverse momentum of the visible subsystem particles. The variable m^{miss} represents the assumed invariant mass of all the invisible particles in the event. The final term in Eq. 1 is a two-vector sum representing the boost correction in the transverse plane caused by upstream processes. In this analysis $\sqrt{s_{min}^{(sub)}}$ is calculated assuming each event arises from $t\bar{t}$ production, with the invisible subsystem comprising one or two neutrinos, and therefore $m^{\text{miss}} = 0$ in Eq. 1. With this assumption, the $\sqrt{s_{min}^{(sub)}}$ distribution for $t\bar{t}$ background events is expected to peak at around $m_{t\bar{t}} = 2m_t \simeq 345$ GeV. On the other hand, stop pair production will peak at lower values if the mass difference between the stop and the neutralino is lower than the top mass, as illustrated in Fig. 1(b) and 1(d). Signal events are therefore selected by imposing an upper limit on $\sqrt{s_{min}^{(sub)}}$.

In the 1-lepton channel, the visible subsystem comprises the single lepton, two light and two b-jets giving the highest estimator in the algorithm described above. In the 2-lepton channel, the two leptons and the two leading jets are used. In both channels, an upper limit on

$\sqrt{s_{min}^{(sub)}}$ has been chosen with a value which maximises the expected signal efficiency with respect to background rejection, across a range of scenarios described in Section 1. In the 1-lepton channel, the optimal requirement found is $\sqrt{s_{min}^{(sub)}} < 250$ GeV, defining a signal region hereafter referred to as 1LSR. In the 2-lepton channel two signal regions are defined, the first requiring $\sqrt{s_{min}^{(sub)}} < 225$ GeV (2LSR1), and the second (tighter) signal region (2LSR2) with $\sqrt{s_{min}^{(sub)}} < 235$ GeV together with an upper limit on the invariant mass of the two leptons and two jets ($m_{\ell\ell jj}$) requiring $m_{\ell\ell jj} < 140$ GeV.

6 Background Estimation

The dominant SM background process in the 1-lepton (2-lepton) channel arises from semi-leptonic (di-leptonic) $t\bar{t}$ decays, comprising 60% (80%) of the total background. The second most significant background in the 1-lepton (2-lepton) channel arises from W (Z/γ^*) production in association with jets from heavy flavour quarks. For both channels, similar methods are used to estimate these backgrounds. For each channel and background process a control region is defined that is rich in the background of interest. The region is kinematically similar to the signal region but distinct from it, such that the signal and control regions have no events in common. For a control region containing N_{CR}^{obs} observed events (corrected for the contamination from other backgrounds), the number of events in the signal region is calculated as $N_{SR} = (N_{SR}^{MC} \times N_{CR}^{obs})/N_{CR}^{MC}$, where N_{SR}^{MC} and N_{CR}^{MC} are the MC-based estimates in the signal and control regions respectively. The advantage of this method is that many systematic uncertainties partially cancel out.

In the 1-lepton channel, the $t\bar{t}$ background is determined with a control region defined by identical cuts to the signal region, except that $\hat{\mu} - 0.5\hat{\sigma} < m_t^{had} < \hat{\mu} + 0.5\hat{\sigma}$ and $\sqrt{s_{min}^{(sub)}} < 320$ GeV, with a $t\bar{t}$ purity of 93%. The definition of a control region using these fitted parameters reduces the systematic uncertainties related to the jet energy scale and resolution. A high-purity W+b-jets control region is more difficult to define due to the kinematic similarity with $t\bar{t}$ events, which have a higher fiducial cross section. A control region can, however, be defined with 38% purity for W events by requiring $m_t^{had} > 250$ GeV and $m_{b\bar{b}} < 50$ GeV. As the $t\bar{t}$ contamination in this region is still relatively high (60%), the W and $t\bar{t}$ contributions are determined simultaneously in both control regions.

In the 2-lepton channel, the $t\bar{t}$ background (including dileptonic Wt decays) is determined using a control region identical to the signal region except that $m_{\ell\ell} > 101$ GeV and $\sqrt{s_{min}^{(sub)}} < 325$ GeV, with 94% purity of $t\bar{t}$ events. The Z background is determined in a region requiring two same-flavour leptons, $81 < m_{\ell\ell} < 101$ GeV and $\sqrt{s_{min}^{(sub)}} < 225$ GeV, with a Z purity of 90%.

The contribution to the background from events where one of the jets is misidentified as a lepton, or where a lepton from a b or c hadron decay is selected (refered to as "fake" lepton background), is estimated using a data-driven technique in both channels [41, 50]. The probability that a jet is misidentified as a lepton is estimated by relaxing the electron and muon identification criteria to obtain control samples dominated by multi-jet production. In the 1-lepton channel, the main contribution is from multi-jet events. In the 2-lepton channel, the dominant contribution is from processes containing one real and one fake lepton, such as W or semi-leptonic $t\bar{t}$ decays. The contribution from events containing two fake leptons was found to be negligible.

Other less significant processes in the 1-lepton channel include Z/γ^*+jets and single top quark production. Dibosons and $t\bar{t} + X$ ($X = W, Z, WW, b\bar{b}$) give a minor contribution to both channels. The contribution to the total background from these processes (referred to as "Oth-
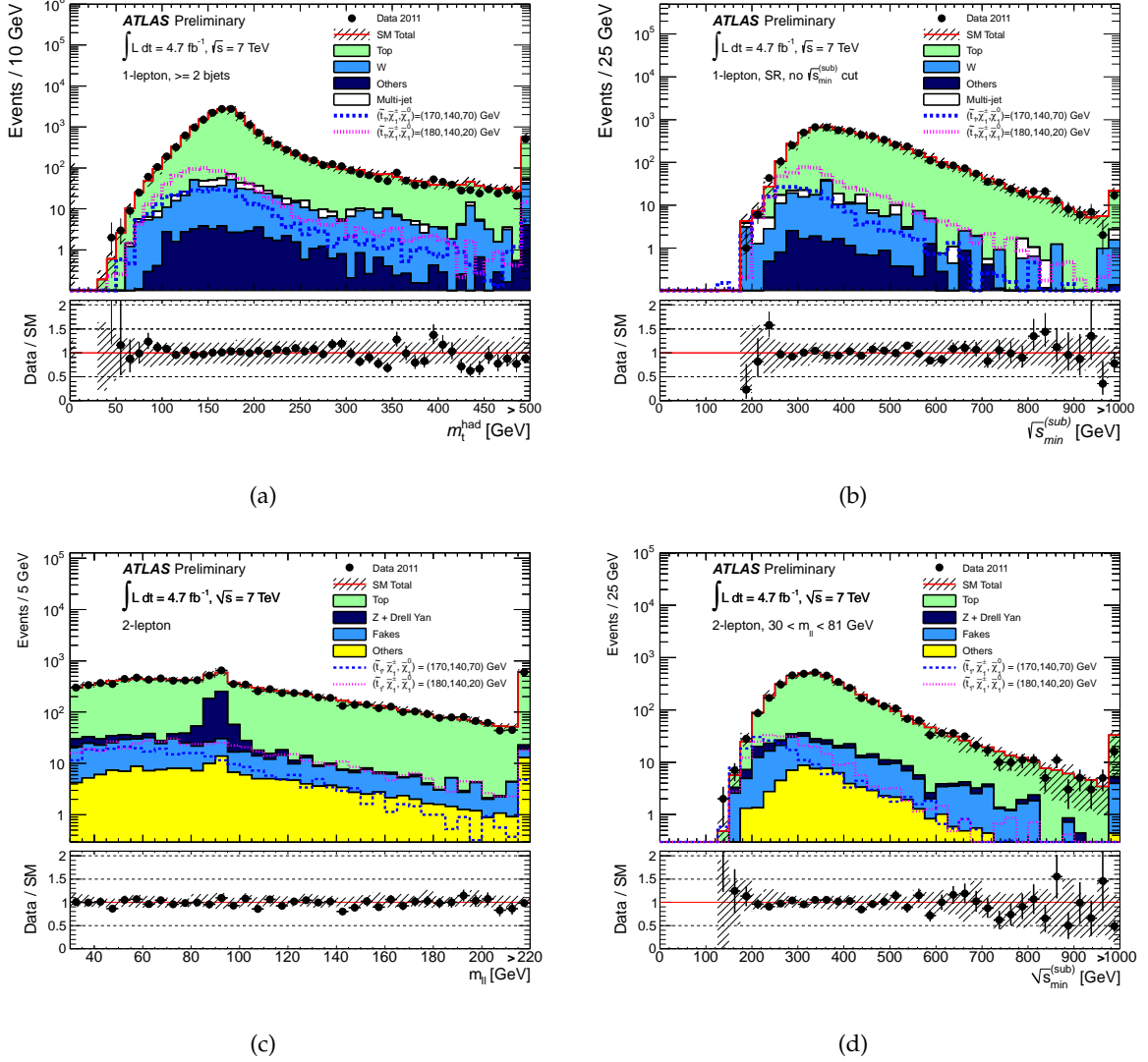
Figure 1: The 1-lepton channel m_t^{had} distribution after all requirements except those on m_t^{had} and $\sqrt{s}_{min}^{(sub)}$ (a), and the $\sqrt{s}_{min}^{(sub)}$ distribution after all requirements except that on $\sqrt{s}_{min}^{(sub)}$ (b). For the 2-lepton channel, the $m_{\ell\ell}$ distribution is shown after all requirements except those on $m_{\ell\ell}$ and $\sqrt{s}_{min}^{(sub)}$ (c), and the $\sqrt{s}_{min}^{(sub)}$ distribution, before the requirements on $\sqrt{s}_{min}^{(sub)}$ itself (d). In all the cases, the MC contributions are normalised to the expected event yield in the corresponding control regions, except in (c), for which no additional normalisation is applied to the Z MC prediction. The hatched bands display the total uncertainties on the background expectation and the final bin in each histogram contains the integral of all events with values greater than the upper axis bound. The dashed lines show the expectations for two signal models with stop (neutralino) masses of 170 (70) and 180 (20) GeV, both with a chargino mass of 140 GeV. The bottom panels show the ratio of data to the expected background (points) and the total uncertainty on the background (hatched area).

ers" in the following and in Fig. 1) is 2.5% (2%) in the 1-lepton (2-lepton) channel, and are taken directly from the MC prediction.

Distributions of $\sqrt{s}_{min}^{(sub)}$ in the 1-lepton control regions can be found in Fig. 2, while the

6

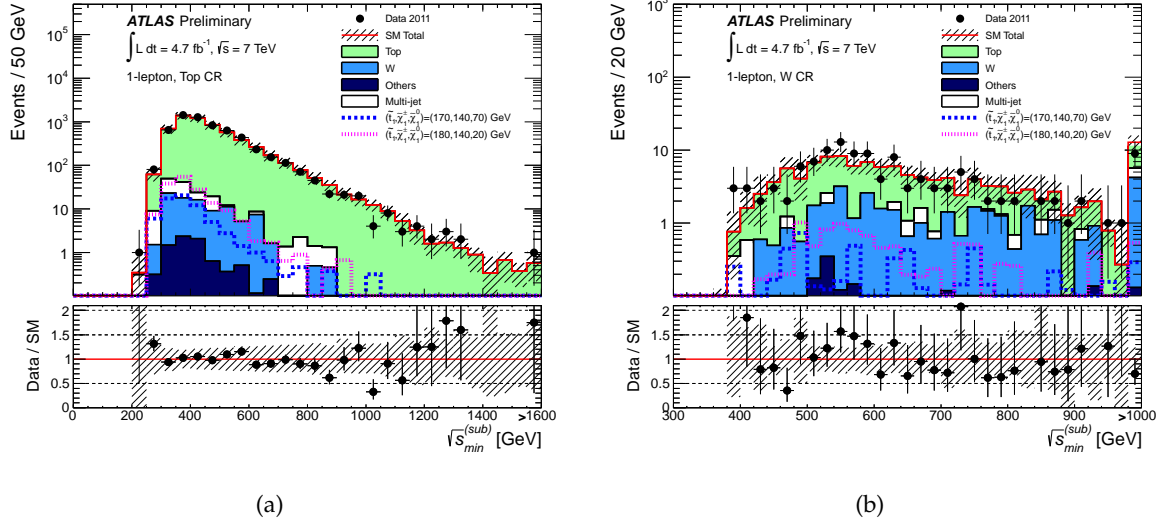Figure 2: The 1-lepton $\sqrt{s}^{(sub)}_{min}$ distributions shown in the top (before the $\sqrt{s}^{(sub)}_{min}$ cut) (a) and W (b) control regions as described in the text. The MC distributions are shown after the normalisation of the $t\bar{t}$ and W contributions to the corresponding control region yields. The hatched bands display the total uncertainties on the background expectation and the final bin in each histogram contains the integral of all events with values greater than the upper axis bound. The dashed lines show the expectations for two signal models with stop (neutralino) masses of 170 (70) and 180 (20) GeV, both with a chargino mass of 140 GeV. The bottom panels show the ratio of data to the expected background (points) and the total uncertainty on the background (hatched area).

corresponding 2-lepton distributions are shown in Fig. 3(a) and 3(b) for the top and Z control regions respectively. Fig. 3(c) also shows the distribution of $m_{\ell\ell jj}$ before the final selection requirements which define 2LSR2.

7 Systematic Uncertainties

The contribution to the systematic uncertainty from the jet energy scale (JES) uncertainty is calculated by shifting the p_T of all jets up and down by p_T and η dependent factors, which vary from 5–3% for jets with p_T from 20–60 GeV. Repeating the analysis with these p_T shifts applied to the MC leads to variations on the final background estimate of 6–10% depending on the signal region. The uncertainty due to the jet energy resolution (JER) is calculated by smearing the p_T of each jet by factors depending on the jet p_T and η. The smearing on a single jet is typically around 10%, and results in an overall uncertainty of 1–10%. Uncertainties in the lepton identification efficiency amount to a 1% systematic uncertainty. The uncertainty on the E_T^{miss} due to the energy scale of calorimeter clusters not associated with jets and electrons is evaluated using the method described in Ref. [51], extended to include dedicated pile-up uncertainties. The effect is up to 9% depending on the signal region. The uncertainty due to b-tagging is evaluated by varying the b-tagging efficiency and mis-tag rates within the uncertainties of the measured values [52,53], giving an effect of 1% in all signal regions. The uncertainty associated with pile-up re-weighting is evaluated by varying the number of interactions per bunch-crossing by 10%. The overall effect on the predicted background yield is at most 3%.
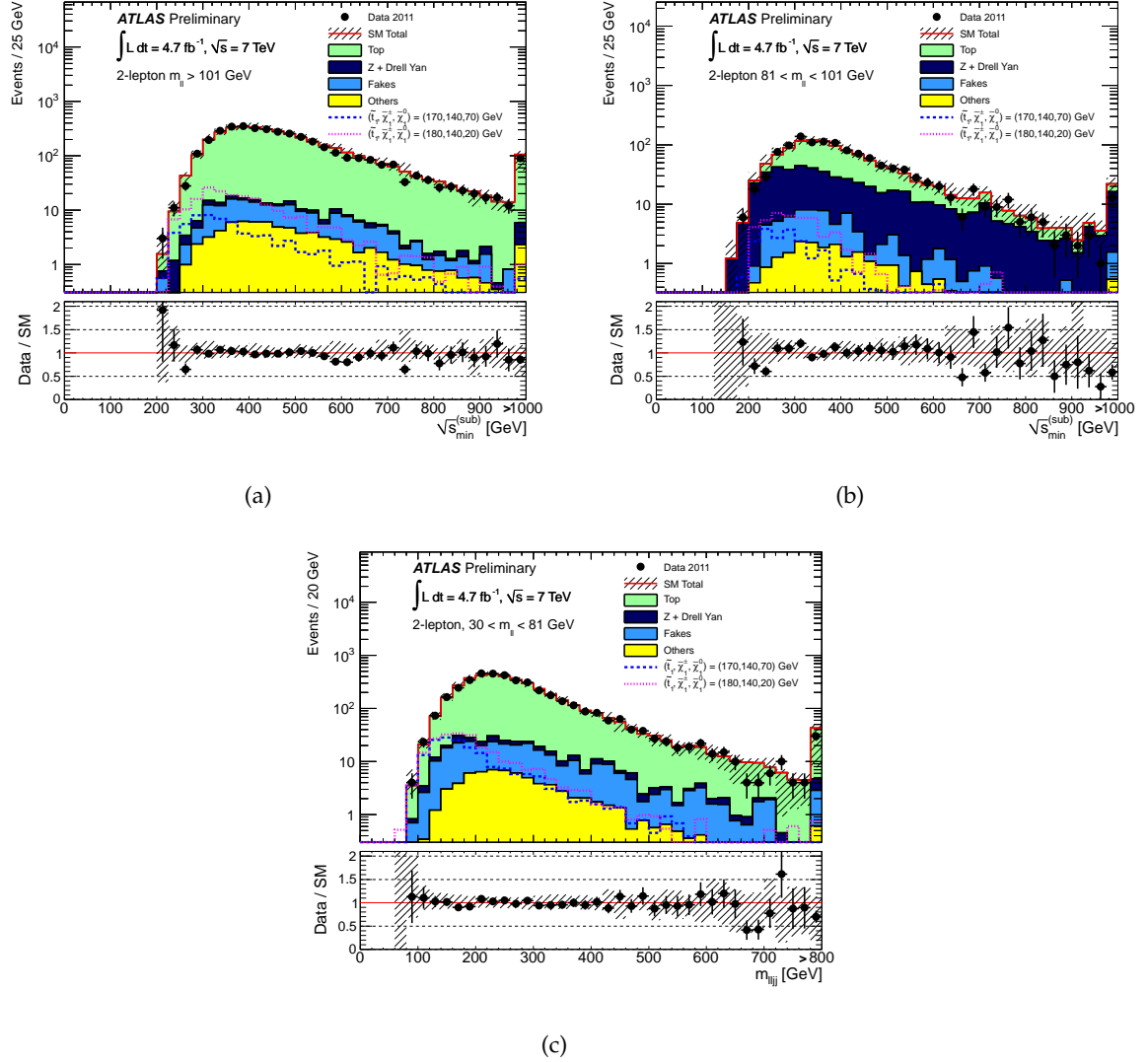
(a)

(b)

(c)

Figure 3: The 2-lepton $\sqrt{s}_{min}^{(sub)}$ regions shown in the top (a) and Z (b) control regions defined in the text, before applying the upper limit on $\sqrt{s}_{min}^{(sub)}$ itself. The $m_{\ell\ell jj}$ distribution is also shown (c) after the requirement $30 < m_{\ell\ell} < 81$ GeV. In all the cases, the top contribution is normalised to the control region yield but the additional Z normalisation is only taken into account in (c). The hatched bands display the total uncertainties on the background expectation and the final bin in each histogram contains the integral of all events with values greater than the upper axis bound. The dashed lines show the expectations for two signal models with stop (neutralino) masses of 170 (70) and 180 (20) GeV, both with a chargino mass of 140 GeV. The bottom panels show the ratio of data to the expected background (points) and the total uncertainty on the background (hatched area).

	Number of events		
Process	1LSR	2LSR1	2LSR2
Top	$24 \pm 3 \pm 5$	$89 \pm 6 \pm 10$	$36 \pm 2 \pm 5$
W+jets	$6 \pm 1 \pm 2$	n/a	n/a
Z+jets	$0.5 \pm 0.3 \pm 0.3$	$11 \pm 4 \pm 3$	$3 \pm 1 \pm 1$
Fake leptons	$7 \pm 1 \pm 2$	$12 \pm 5 \pm 11$	$6 \pm 4 \pm 4$
Others	$0.3 \pm 0.1 \pm 0.1$	$2.7 \pm 0.9 \pm 0.7$	$0.9 \pm 0.2 \pm 0.5$
Total SM	$38 \pm 3 \pm 7$	$115 \pm 8 \pm 15$	$46 \pm 4 \pm 7$
Data	50	123	47
$m_{\tilde{t}_1} = 170$ GeV, $m_{\tilde{\chi}_1^0} = 70$ GeV	$26 \pm 2 \pm 6$	$57 \pm 3 \pm 6$	$36 \pm 2 \pm 4$
$m_{\tilde{t}_1} = 180$ GeV, $m_{\tilde{\chi}_1^0} = 20$ GeV	$20 \pm 2 \pm 4$	$41 \pm 3 \pm 5$	$27 \pm 2 \pm 3$
	95% CL upper limits		
σ_{vis} (expected) [fb]	4.2	9.3	4.6
σ_{vis} (observed) [fb]	6.1	11	5.2

Table 1: Predicted and observed number of events in all signal regions together with their statistical and systematic uncertainties. No values are shown for the W+jets contribution in the 2-lepton channel as these are included in the fake contribution. The expected number of events for two signal scenarios, both with a chargino mass of 140 GeV, are also shown. The observed and expected upper limits at 95% confidence level on $\sigma_{\text{vis}} = \sigma \cdot A \cdot \varepsilon$ are also given.

Theoretical uncertainties on the $t\bar{t}$ background due to the choice of generator are evaluated by comparing event yields from MC@NLO to those from POWHEG with the same parton shower model (HERWIG). The parton shower uncertainties are then calculated by comparing samples generated with the HERWIG and PYTHIA parton shower models, with the same generator (POWHEG). The uncertainty due to ISR/FSR is assessed using AcerMC samples with variations of PYTHIA parameters related to the ISR branching phase-space and the FSR low-p_{T} cutoff. These variations are chosen to produce jet activity in $t\bar{t}$ events that is consistent with the data [54, 55]. The total uncertainty on the $t\bar{t}$ estimate due to these effects amounts to 10–15%. Uncertainties due to the PDF choice and errors are found to be negligible.

In the 1-lepton channel, the theoretical uncertainty in the W estimate due to variations of the factorisation, renormalisation and matching scales is found to be 15%. Similar uncertainties on the Z/γ^* contribution in the 2-lepton channel are 9% (2%) in 2LSR1 (2LSR2).

Uncertainties on the data-driven background from fake leptons arise from the lepton fake rate determination and from the definition of the fake-enriched control regions. The effect is between 45–84% of the fake contribution.

Theoretical uncertainties on stop pair production are calculated as described in Section 3. Signal uncertainties related to the JES, JER and b-tagging are treated as fully correlated with the respective background uncertainties. Finally, the luminosity uncertainty is 3.9%.

8 Results and Interpretation

Table 1 reports the observed number of events in data and the SM predictions for the signal regions of the 1- and 2-lepton channels. In all SRs, the data are in good agreement with the SM expectations. Fig. 1 shows the observed m_t^{had} and $\sqrt{s}_{min}^{(sub)}$ ($m_{\ell\ell}$ and $\sqrt{s}_{min}^{(sub)}$) distributions for the 1-lepton (2-lepton) channels compared to the SM predictions. MC estimates for these predictions are used, where the total prediction and systematic uncertainty are scaled to match

the results obtained from the top and W+jets (Z+jets) 1-lepton (2-lepton) control regions. The expected distributions for two MSSM scenarios are also shown for illustrative purposes.

The results are translated into 95% confidence-level (CL) upper limits on contributions from new physics using the CL_s prescription [56]. The three signal regions are used to set limits on the visible cross section[2] of new physics models, as shown in Table 1. Results are interpreted in the MSSM scenarios described in Section 1. Fig. 4 presents the expected and observed limits, using a combination of 1LSR and the best expected limit from either 2LSR1 or 2LSR2. The effect of signal contamination in the control regions (typically 5–10% depending on the signal point) is taken into account. In the gaugino universality scenario, stop masses from 120 GeV up to the top mass are excluded for $m_{\tilde{\chi}_1^0} = 55$ GeV. The sensitivity of the search is also evaluated for a stop mass of 180 GeV whilst varying the chargino-neutralino mass difference. In the scenario with $m_{\tilde{\chi}_1^\pm} = 106$ GeV, stop masses are excluded from 120 GeV up to the top mass for $m_{\tilde{\chi}_1^0} = 55$ GeV. Neutralino masses of 75 GeV are excluded for $130 < m_{\tilde{t}_1} < 155$ GeV.

9 Conclusions

A search has been performed for top squarks with masses near or lower than the top quark mass. Good agreement is observed between data and the SM predictions in all channels. The results allow limits to be set in the $\tilde{t}_1 - \tilde{\chi}_1^0$ mass plane. In the two MSSM scenarios considered, stop masses from 120 GeV up to the top mass are excluded for $m_{\tilde{\chi}_1^0} = 55$ GeV.

---

[2]The visible cross section, σ_{vis}, is defined by the product of the new physics production cross section, acceptance A and efficiency ε.
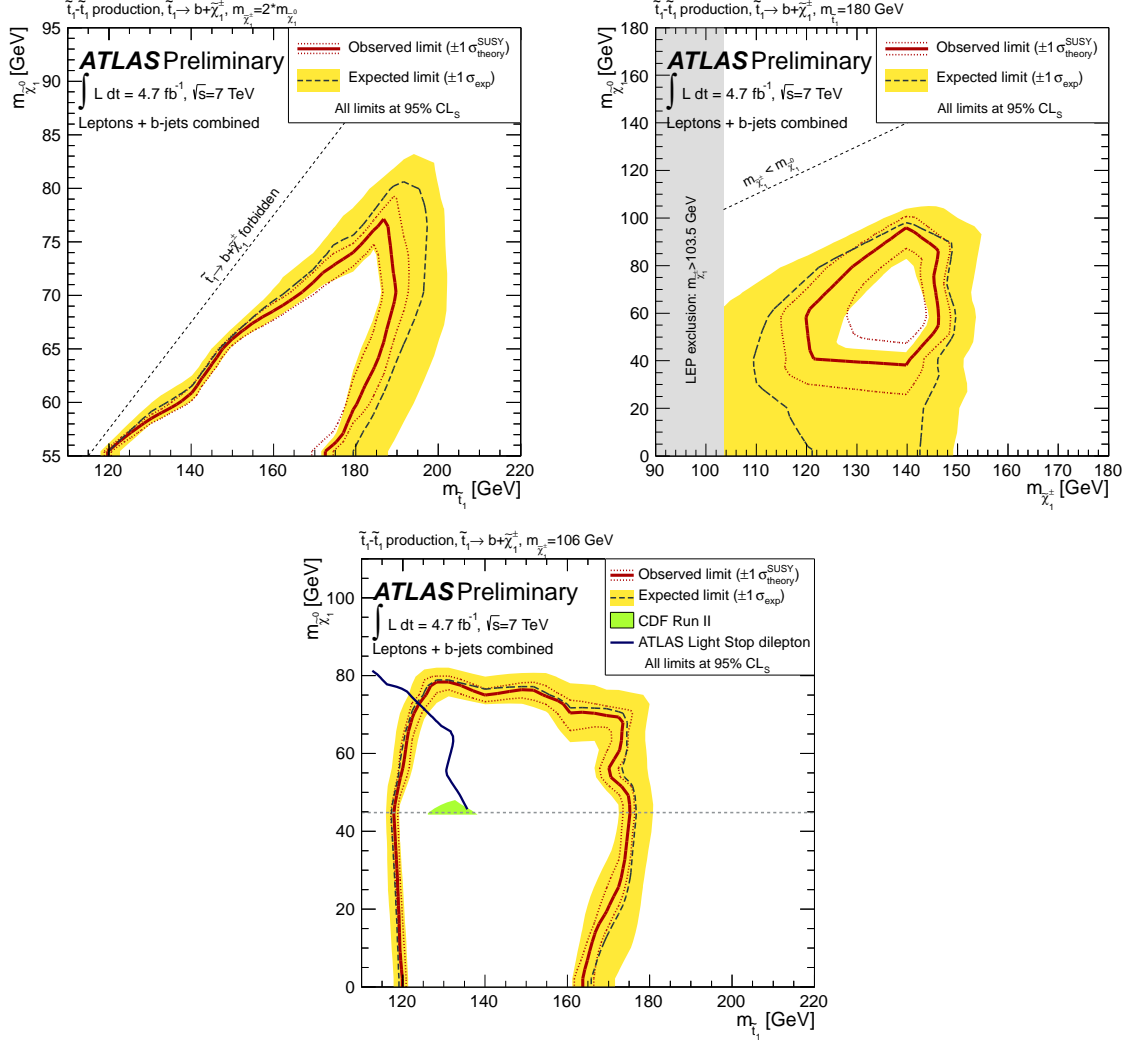
Figure 4: Exclusion limits at 95% CL for the three scenarios described in the text. The dashed black and solid red lines show the expected and observed limits, respectively, including all uncertainties except for the theoretical signal cross section uncertainty (PDF and scale). The yellow bands around the expected limits show the $\pm 1\sigma$ results. The lines around the observed limits represent the results obtained when moving the nominal signal cross section up or down by the $\pm 1\sigma$ theoretical uncertainty. For the scenarios at fixed chargino mass, results are compared to previous exclusion limits from the Tevatron and ATLAS experiments, where the lowest neutralino mass considered was $m_{\tilde{\chi}_1^0} = 45$ GeV, indicated by the horizontal dotted line.

References

[1] H. Miyazawa, *Baryon Number Changing Currents*, Prog. Theor. Phys. **36 (6)** (1966) 1266–1276.

[2] R. Ramond, *Dual Theory for Free Fermions*, Phys. Rev. **D3** (1971) 2415–2418.

[3] Y. A. Golfand and E. P. Likhtman, *Extension of the Algebra of Poincare Group Generators and Violation of p Invariance*, JETP Lett. **13** (1971) 323–326. [Pisma Zh.Eksp.Teor.Fiz.13:452-455,1971].

[4] A. Neveu and J. H. Schwarz, *Factorizable dual model of pions*, Nucl. Phys. **B31** (1971) 86–112.

[5] A. Neveu and J. H. Schwarz, *Quark Model of Dual Pions*, Phys. Rev. **D4** (1971) 1109–1111.

[6] J. Gervais and B. Sakita, *Field theory interpretation of supergauges in dual models*, Nucl. Phys. **B34** (1971) 632–639.

[7] D. V. Volkov and V. P. Akulov, *Is the Neutrino a Goldstone Particle?*, Phys. Lett. **B46** (1973) 109–110.

[8] J. Wess and B. Zumino, *A Lagrangian Model Invariant Under Supergauge Transformations*, Phys. Lett. **B49** (1974) 52.

[9] J. Wess and B. Zumino, *Supergauge Transformations in Four-Dimensions*, Nucl. Phys. **B70** (1974) 39–50.

[10] P. Fayet, *Supersymmetry and Weak, Electromagnetic and Strong Interactions*, Phys. Lett. **B64** (1976) 159.

[11] P. Fayet, *Spontaneously Broken Supersymmetric Theories of Weak, Electromagnetic and Strong Interactions*, Phys. Lett. **B69** (1977) 489.

[12] G. R. Farrar and P. Fayet, *Phenomenology of the Production, Decay, and Detection of New Hadronic States Associated with Supersymmetry*, Phys. Lett. **B76** (1978) 575–579.

[13] P. Fayet, *Relations Between the Masses of the Superpartners of Leptons and Quarks, the Goldstino Couplings and the Neutral Currents*, Phys. Lett. **B84** (1979) 416.

[14] S. Dimopoulos and H. Georgi, *Softly Broken Supersymmetry and SU(5)*, Nucl. Phys. **B193** (1981) 150.

[15] M. Carena, G. Nardini, M. Quiros, and C. E. Wagner, *The Effective Theory of the Light Stop Scenario*, JHEP **0810** (2008) 062.

[16] M. Carena, G. Nardini, M. Quiros, and C. Wagner, *The Baryogenesis Window in the MSSM*, Nucl. Phys. **B812** (2009) 243–263.

[17] LEP SUSY Working Group (ALEPH, DELPHI, L3, OPAL), Notes LEPSUSYWG/01-03.1 and 04-01.1, http://lepsusy.web.cern.ch/lepsusy/Welcome.html.

[18] CDF Collaboration, *Search for Pair Production of Supersymmetric Top Quarks in Dilepton Events from $p\bar{p}$ Collisions at $\sqrt{s}$ = 1.96 TeV*, Phys. Rev. Lett. **104** (2010) 251801.

[19] ATLAS Collaboration, *Search for light scalar top quark pair production in final states with two leptons with the ATLAS detector in* $\sqrt{s} = 7$ *TeV proton–proton collisions*, ATLAS-CONF-2012-059, https://cdsweb.cern.ch/record/1453787.

[20] ATLAS Collaboration, *The ATLAS Experiment at the CERN Large Hadron Collider*, JINST **3** (2008) S08003.

[21] S. Frixione, B. R. Webber, JHEP 06 (2002) 029; S. Frixione, P. Nason and B. R. Webber, JHEP 08 (2003) 007; S. Frixione, E. Laenen and P. Motylinski, JHEP 03 (2006) 092.

[22] P. M. Nadolsky et al., *Implications of CTEQ global analysis for collider observation*, Phys. Rev. **D78** (2008) 013004, arXiv:0802.0007 [hep-ph].

[23] M. L. Mangano, M. Moretti, F. Piccinini, R. Pittau, and A. D. Polosa, *ALPGEN, a generator for hard multiparton processes in hadronic collisions*, JHEP **07** (2003) 001.

[24] J. Alwall, M. Herquet, F. Maltoni, O. Mattelaer, and T. Stelzer, *MadGraph 5 : Going Beyond*, JHEP **1106** (2011) 128, arXiv:1106.0522 [hep-ph].

[25] T. Sjostrand, S. Mrenna, and P. Skands, *PYTHIA 6.4 physics and manual*, JHEP **05** (2006) 026.

[26] G. Corcella et al., *HERWIG 6: An event generator for hadron emission reactions with interfering gluons (including supersymmetric processes)*, JHEP **01** (2001) 010.

[27] B. P. Kersevan and E. Richter-Was, *The Monte Carlo event generator AcerMC version 2.0 with interfaces to PYTHIA 6.2 and HERWIG 6.5*, 2004. arXiv:hep-ph/0405247.

[28] J. F. J. Butterworth and M. Seymour, *Multiparton interactions in photoproduction at HERA*, Z. Phys. **C72** (1996) 637–646.

[29] S. Frixione, P. Nason, and C. Oleari, *Matching NLO QCD computations with Parton Shower similations: the POWHEG method*, JHEP **11** (2007) 070.

[30] A. Sherstnev and R. Thorne, *Parton Distributions for LO Generators*, Eur. Phys. J. **C55** (2008) 553–575, arXiv:0711.2473 [hep-ph].

[31] J. Pumplin et al., *New generation of parton distributions with uncertainties from global QCD analysis*, JHEP **0207** (2002) 012, arXiv:hep-ph/0201195 [hep-ph].

[32] ATLAS Collaboration, *Search for supersymmetry in pp collisions at* $\sqrt{s} = 7$ *TeV in final states with missing transverse momentum and b-jets with the ATLAS detector*, Phys.Rev. **D85** (2012) 112006, arXiv:1203.6193 [hep-ex].

[33] M. Bahr et al., *Herwig++ Physics and Manual*, Eur. Phys. J. **C58** (2008) 639–707.

[34] W. Beenakker, M. Kramer, T. Plehn, M. Spira, and P. M. Zerwas, *Stop production at hadron colliders*, Nucl. Phys. **B515** (1998) 3–14.

[35] W. Beenakker, S. Brensing, M. Kramer, A. Kulesza, E. Laenen, and I. Niessen, *Supersymmetric top and bottom squark production at hadron colliders*, JHEP. **1008** (2010) 098.

[36] W. Beenakker, S. Brensing, M. Kramer, A. Kulesza, E. Laenen, et al., *Squark and gluino hadroproduction*, Int. J. Mod. Phys. **A26** (2011) 2637–2664.

[37] M. Kramer, A. Kulesza, R. van der Leeuw, M. Mangano, S. Padhi, et al., *Supersymmetry production cross sections in pp collisions at $\sqrt{s}$ = 7 TeV*, `arXiv:1206.2892 [hep-ph]`.

[38] ATLAS Collaboration, ATL-PHYS-PUB-2010-014
`https://cdsweb.cern.ch/record/1303025` (2010) and ATLAS-CONF-2010-031
`https://cdsweb.cern.ch/record/1277665` (2010).

[39] GEANT4 Collaboration, S. Agostinelli et al., *GEANT4: A simulation toolkit*, Nucl. Instrum. Meth. **A506** (2003) 250–303.

[40] ATLAS Collaboration, *The ATLAS Simulation Infrastructure*, Eur. Phys. J. **C70** (2010) 823–874.

[41] ATLAS Collaboration, *Electron performance measurements with the ATLAS detector using the 2010 LHC proton-proton collision data*, Eur. Phys. J. **C72** (2012) 1909.

[42] ATLAS Collaboration, *Muon reconstruction efficiency in reprocessed 2010 LHC p-p collision data recorded with the ATLAS detector*, ATLAS-CONF-2011-063 (2011)
`https://cdsweb.cern.ch/record/1345743`.

[43] M. Cacciari, G. P. Salam, and G. Soyez, *The anti-k_T jet clustering algorithm*, JHEP **04** (2008) 063.

[44] ATLAS Collaboration, *Jet energy measurement with the ATLAS detector in proton-proton collisions at $\sqrt{s}$ = 7 TeV*, `arXiv:1112.6426 [hep-ex]`. Submitted to Eur. Phys. J. C.

[45] ATLAS Collaboration, *Commissioning of the ATLAS high-performance b-tagging algorithms in the 7 TeV collision data*, ATLAS-CONF-2011-102, 2010.
`https://cdsweb.cern.ch/record/1369219`.

[46] ATLAS Collaboration, *Luminosity Determination in pp Collisions at $\sqrt{s}$=7 TeV Using the ATLAS Detector at the LHC*, Eur.Phys.J. **C71** (2011) 1630, `arXiv:1101.2185 [hep-ex]`.

[47] ATLAS Collaboration, *Luminosity Determination in pp Collisions at $\sqrt{s}$ = 7 TeV using the ATLAS Detector in 2011*, ATLAS-CONF-2011-116
`http://cdsweb.cern.ch/record/1376384` (2011).

[48] Particle Data Group Collaboration, K. Nakamura et al. J. Phys. **G37** (2010) 075021.

[49] P. Konar, K. Kong, K. T. Matchev, and M. Park, *RECO level $\sqrt{s}_{min}$ and subsystem $\sqrt{s}_{min}$: Improved global inclusive variables for measuring the new physics mass scale in E_T events at hadron colliders*, JHEP **1106** (2011) 041.

[50] ATLAS Collaboration, *Searches for supersymmetry with the ATLAS detector using final states with two leptons and missing transverse momentum in $\sqrt{s}$ = 7 TeV proton-proton collisions*, Phys.Lett. **B709** (2012) 137–157.

[51] ATLAS Collaboration, *Performance of Missing Transverse Momentum Reconstruction in Proton-Proton Collisions at 7 TeV with ATLAS*, Eur. Phys. J. **C72** (2012) 1844.

[52] ATLAS Collaboration, *Observation of energetic jets in pp collisions at $\sqrt{s}$ = 7 TeV using the ATLAS experiment at the LHC*, ATLAS-CONF-2010-043, June, 2010.
`https://cdsweb.cern.ch/record/1277683`.

[53] ATLAS Collaboration, *Measurement of the Mistag Rate of b-tagging algorithms with 5 fb^{-1} of Data Collected by the ATLAS Detector*, ATLAS-CONF-2012-040, 2012. `https://cdsweb.cern.ch/record/1435194`.

[54] ATLAS Collaboration, *Measurement of $t\bar{t}$ production with a veto on additional central jet activity in pp collisions at $\sqrt{s}$ = 7 TeV using the ATLAS detector*, `arXiv:1203.5015` `[hep-ex]`.

[55] ATLAS Collaboration, *ATLAS tunes of PYTHIA 6 and Pythia 8 for MC11*, ATL-PHYS-PUB-2011-009. `https://cdsweb.cern.ch/record/1363300`.

[56] A. L. Read, *Presentation of search results: The CL(s) technique*, J. Phys. **G28** (2002) 2693–2704.